Electronic Supplementary Information

Direct synthesis of highly porous interconnected carbon nanosheets from sodium D-Isoascorbic acid for simultaneous determination of catechol and hydroquinone

Yin Zheng [a], Jiabing Chen [a, b], Youluan Lu [a, b], Xinjian Song [*, b], Zhen Shi [b]

[a] *Key Laboratory of Green Manufacturing of Super-light Elastomer Materials of State Ethnic Affairs Commission，Hubei Minzu University, Enshi 445000, China.*

[b] *School of Chemical and Environmental Engineering, Hubei Minzu University, Enshi 445000, China.*

Table S1 Comparison of analytical characteristics of the SDAIPC-900/GCE for the simultaneous determination of HQ and CA.

Entry	Electrode materials	Analytes	Linear range (μmol/L)	Detection limit (μmol/L)	References
1	Graphene quantum dots/GCE	HQ	4-600	0.4	1
		CA	6-400	0.75	
2	graphene–chitosan composite/GCE	HQ	1-400	0.75	2
		CA	1-300	0.37	
3	CNCs-RGO/GCE	HQ	1-400	0.87	3
		CA	1-300	0.4	
4	GMC/BMIMPF6/GCE	HQ	0.1-50	0.05	4
		CA	0.1-50	0.06	
5	Nafion/MWCNTs/CDs/MWCNTs/GCE	HQ	1-200	0.07	5
		CA	4-200	0..06	
6	CMK-$_3$/MWCNTs/GCE	HQ	0.5-35	0.1	6
		CA	1-35	0.1	
7	Boron-doped graphene/GCE	HQ	5-100	0.3	7
		CA	1-75	0.2	
8	SDAIPC-900/GCE	HQ	0.4-20	0.028	This work
		CA	0.4-20	0.032	

Table S2 Determination of HQ and CA in real samples.

Sample	Analytes	Added (μmol/L)	Found (μmol/L)	Recovery (%)	RSD (%)
1	HQ	1	0.963	96.3	3.1
	CA	1	0.968	96.8	2.7
2	HQ	5	5.12	102.4	4.2
	CA	5	4.87	97.4	3.6
3	HQ	15	14.80	98.7	2.5
	CA	15	15.24	101.6	3.5

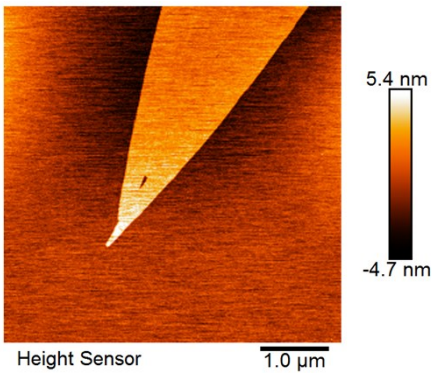

Fig. S1. AFM images of SDAIPC-900.

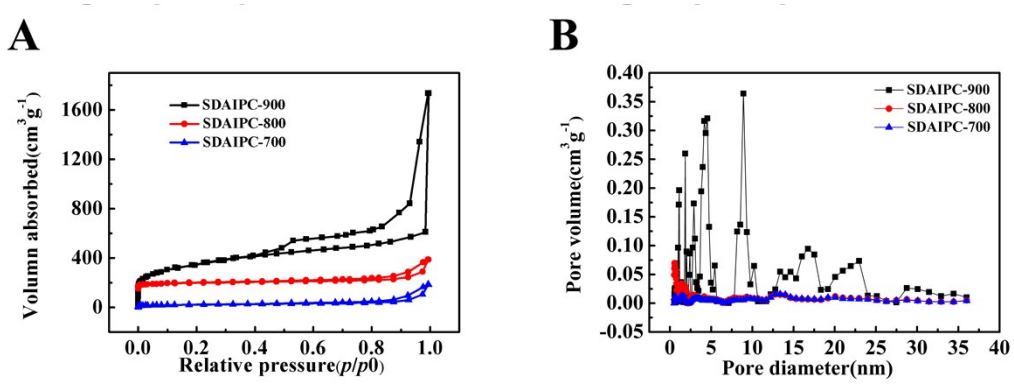

Fig. S2. N_2 adsorpition-desorpition isotherm (A) and pore size distribution (B) of SDAIPC-X.

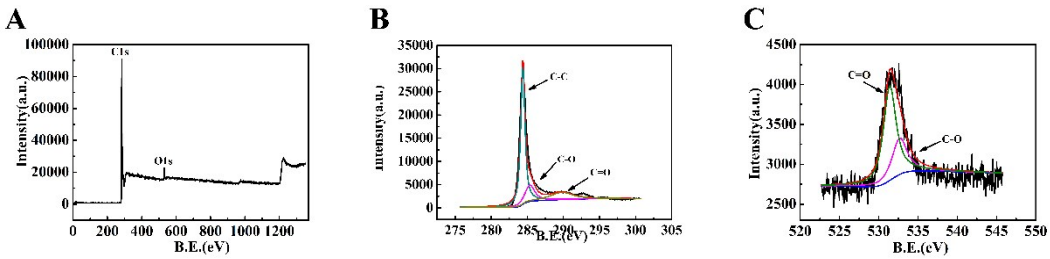

Fig. S3. XPS spectra for SDAIPC-900 (A) and high-resolution XPS spectra of C1s (B), O1s for the SDAIPC-900 (C).

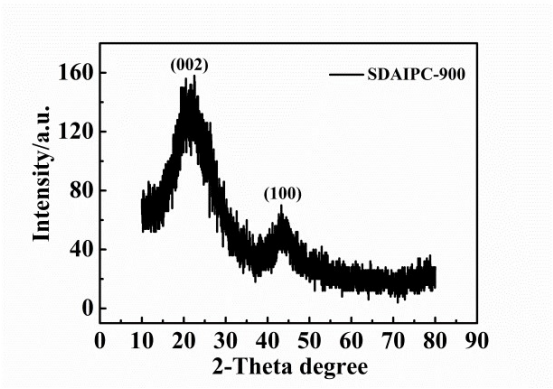

Fig. S4. XRD pattern of SDAIPC-900.

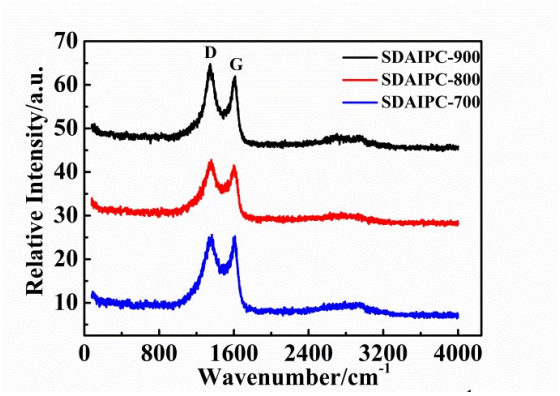

Fig. S5. Raman spectra of SDAIPC-700, SDAIPC-800 and SDAIPC-900.

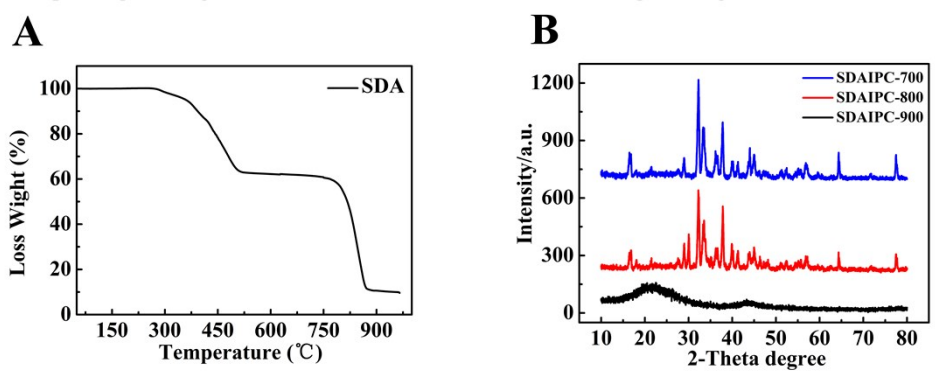

Fig. S6 (A) TGA profile of Sodium D-Isoascorbic acid (Ar atmosphere, heating rate of 10 °C/min); **(B)** XRD patterns for SDAIPC-700, SDAIPC-800 and SDAIPC-900.

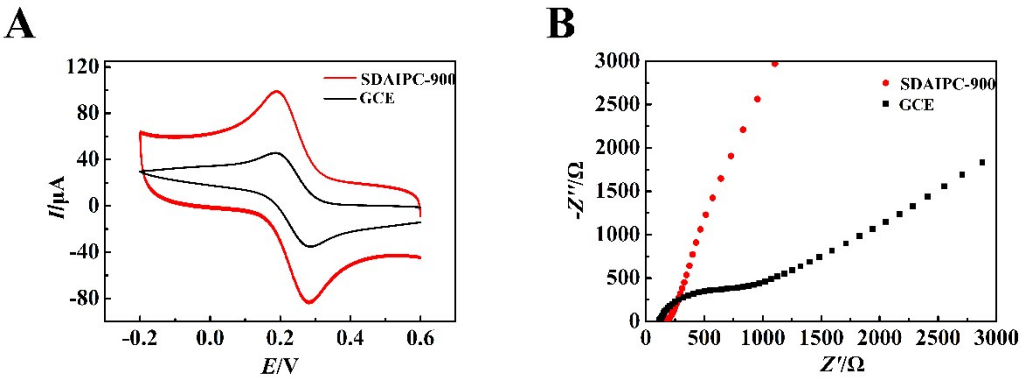

Fig. S7. Cyclic voltammograms (A) and Nyquist plots (B) obtained at a SDAIPC-900/GCE in 0.1 mol/L KCl containing 5 mmol/L $K_3Fe(CN)_6/K_4Fe(CN)_6$ (1:1). Frequency is over the range from 1.0×10^5 to 1.0×10^{-2} Hz.

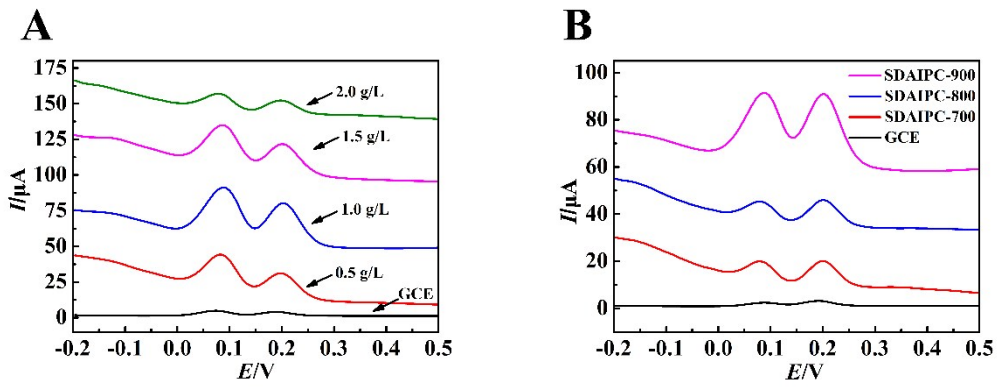

Fig. S8. Influences of modification concentration (A) and pyrolysis temperature (B).

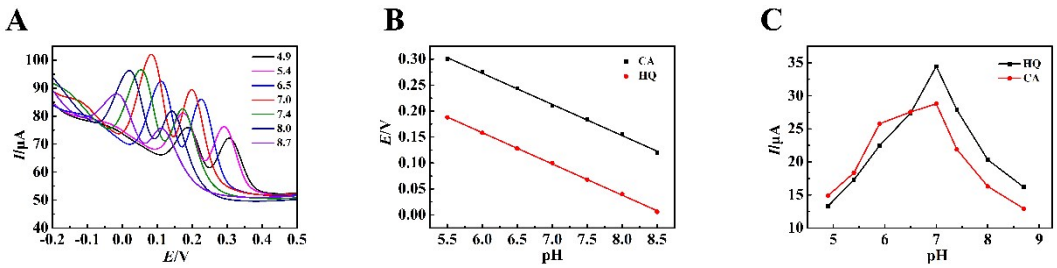

Fig. S9. Influences of pH values on the oxidation peak currents of 10 μM HQ and 10 μM CA at SDAIPC-900/GCE.

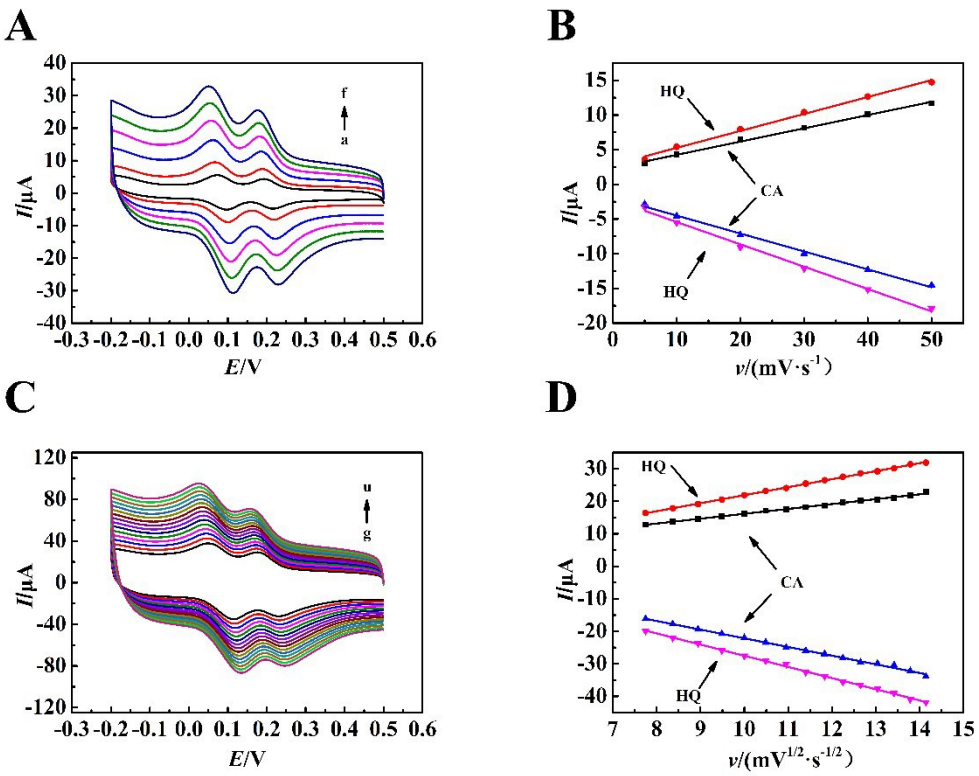

Fig. S10. CV curves in scan rates range of 5-50 (A) (a→f: 5, 10, 20, 30, 40, 50 mV/s) and scan rates range of 60-200 mV/s (C) (g→u: 60, 70, 80, 90, 100, 110, 120, 130, 140, 150, 160, 170, 180, 190, 200 mV/s) in the presence of 10 μM HQ and 10 μM CA, linear relationships between the peak current of HQ and CA and the scan rate (B) and the square root of the scan rate (D).

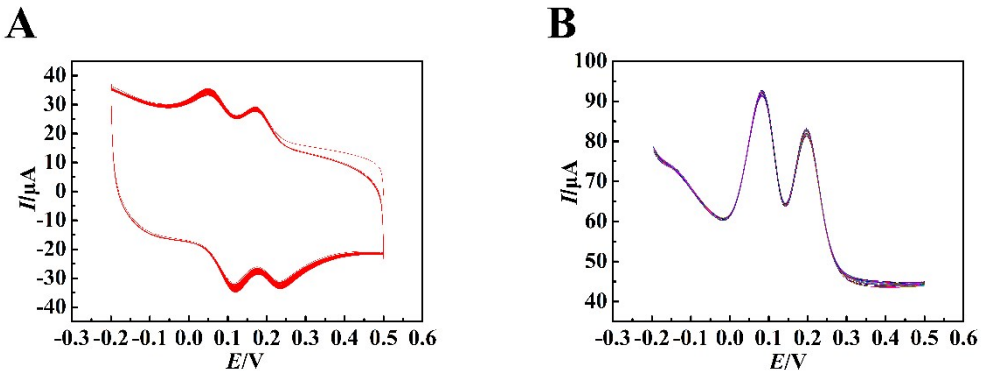

Fig. S11. Cyclic voltammograms (A) and DPV curves (B) for repeated measurements with SDAIPC-900/GCE in the presence of 10 μM HQ and 10 μM CA

with 30 cycles.

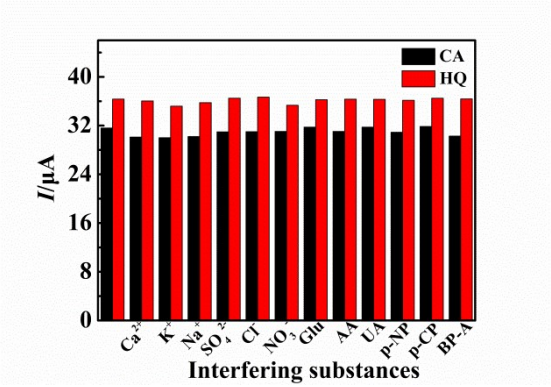

Fig. S12. Influences of different interfering substances on oxidation peak currents in the presence of 10 μM HQ and 10 μM CA at SDAIPC-900/GCE.

Some works have been repored of interconnected porous carbons derived from organic salts and the application in double-layer rubidium capacitors and lithium ion batteries. These porous carbon-derived organic salts include sodium gluconate, sodium alginate, potassium citrate, and sodium glutamate. However, the carbon derived by organic salt used in electroanalysis was rarely reported. SDAIPC-900 can be used as electrochemical materials for simultaneous detection of HQ and CA mainly owing to its huge specific surface area and abundant pores, which provides more active sites for HQ and CA to provide larger electrochemical signals. The large specific surface area was mainly provided by the pleated carbon nanosheets and abundant pores. The doping of O also provided hydrogen bonding for HQ and CA on the nanosheets. The interconnection network formed by the porous structure not only shortens the ion transfer distance, but also improves the electron transfer rate, which was beneficial to the transmission of electrochemical signals.

References

1. X. Jian, X. Liu, H. M. Yang, M. M. Guo, X. L. Song, H. Y. Dai and Z. H. Liang, *Electrochim. Acta*, 2016, **190**, 455–462.
2. H. S. Yin, Q. M. Zhang, Y. L. Zhou, Q. Ma, T. Liu, L. S. Zhu and S. Y. Ai, *Electrochim. Acta*, 2011, **56**, 2748–2753.
3. Y. H. Huang, J. H. Chen, X. Sun, Z. B. Su, H. T. Xing, S. R. Hu, W. Weng, H. X. Guo, W. B. Wu and Y. S. He, *Sens. Actuators, B*, 2015, **212**, 165–173.
4. Z. Q. Hong, L. H. Zhou, J. X. Li and J. Tang, *Electrochim. Acta*, 2013, **109**, 671–677.
5. C. Wei, Q. T. Huang, S. R. Hu, H. Q. Zhang, W. X. Zhang, Z. M. Wang, M. L. Zhu, P. W. Dai and L. Z. Huang, *Electrochim. Acta*, 2014, **149**, 237–244.
6. J. Yu, W. Du, F. Zhao and B. Z. Zeng, *Electrochim. Acta*, 2009, **54**, 984.
7. Y. Z. Zhang, R. X. Sun, B. M. Luo and L. J. Wang, *Electrochim. Acta*, 2015, **156**, 228–234.